Observer Quality as a Resource Variable in Quantum Darwinism: Optimal Decoding, ε-Approximate Spectrum Broadcast Structure, and a Central-Spin Worked Example

Alia Wu
Risk Efficacy & Redline Rising
wut08@nyu.edu
ORCID: 0009-0005-4424-102X

February 7, 2026

Abstract

Quantum Darwinism (QD) and Spectrum Broadcast Structure (SBS) formalize a mechanism by which many observers can learn the same classical pointer value of a system by measuring different fragments of its environment. Most QD analyses treat the observer as idealized: unlimited access, perfect calibration, and no temporal constraints. This paper introduces an explicit *observer quality* parameterization and propagates it through redundancy and objectivity statements in a way that remains stable under an explicit ε-SBS trace-distance error model.

Our main technical contributions are: (i) a decoder-level, tight (Chernoff-optimal) sample-complexity characterization for the number of environmental fragments needed to infer a pointer value under a calibrated observer model, (ii) a data-processing theorem showing that calibration noise (modeled as a CPTP channel) degrades the quantum Chernoff exponent, and (iii) an ε-robustness theorem upgrading ideal-SBS sample-complexity bounds to approximate-SBS states with additive error control.

To address "no concrete physics" concerns, we provide a fully worked open-system example: a central-spin pure-dephasing model whose conditional fragment states can be computed analytically, yielding explicit formulas for the observer parameters (R_O, Λ_O, τ_O) (where a scalar calibration index C_O is derived from Λ_O for binary tasks) as functions of couplings, readout noise, and acquisition time. We also highlight a sharp performance gap between collective (coherent) decoding and commonly used fixed per-fragment readouts (e.g., repeated single-copy Helstrom measurements) for pure-state records, directly linking *quantum memory horizon* to redundancy. Finally, we show that the conditional-independence structure of SBS states is a bipartite factor DAG whose latent node is the pointer variable, instantiating the belief-dependency graph of the Dot–Linear–Network (DLN) compression framework without modification. This identification yields a three-stage decoder classification $q_O \in \{q_{\mathrm{D}}, q_{\mathrm{L}}, q_{\mathrm{N}}\}$ with a tight, achievable factor-of-two exponent gap between product and collective decoding for pure-state records, and a revision-graph formalism governing adaptive transitions between measurement strategies under changing coherence conditions. We also demonstrate *inverted sophistication*: an unmonitored collective decoder can be strictly outperformed by product decoding when coherence reliability falls below a critical threshold, and show that this inversion requires observer-side rather than system-side decoherence.

1 Introduction

Quantum Darwinism proposes that classical objectivity arises when information about a preferred pointer observable of a system is redundantly encoded in the environment [1–3]. A complementary structural characterization is Spectrum Broadcast Structure [4, 5], and strong-QD variants connect entropic and geometric criteria [5, 6].

A persistent modeling gap is that *observers are usually treated as ideal*. Yet in realistic experiments or cognitive settings, an observer may: (i) access only a fraction of environment fragments, (ii) have imperfect measurement calibration, and (iii) be limited by a temporal integration horizon (finite memory or pointer stability). There is substantial prior work on non-idealities in the *environment* (e.g., "hazy" environments [7]) and on generic emergence of objectivity [8, 9], but the observer itself is rarely parameterized at the same level of explicitness.

Scope of this paper. We restrict to a single core task: *observer-relative redundancy/objectivity statements* in QD/SBS when the observer is explicitly modeled by a quality triple

$$Q_O = (R_O, \Lambda_O, \tau_O),$$

where R_O is an access fraction, Λ_O is a calibration channel applied to each accessed fragment prior to readout, and τ_O is an acquisition or memory horizon. For interpretability (and to align with existing QD language) we also extract a scalar *calibration index* C_O from Λ_O in the binary case.

Why an ε-SBS error model. Many QD/SBS derivations assume conditional i.i.d. record models. Instead, we start from an explicit trace-distance approximation: the actual joint state $\rho_{S\mathcal{E}}$ is within ε in trace distance of an *ideal* SBS state $\sigma_{S\mathcal{E}}$. We then push sample-complexity statements through this approximation using data processing and decision-theoretic continuity bounds.

2 Related work and positioning

This paper builds on three strands:

1. **QD and SBS foundations.** The environment-as-witness framing originates in Ollivier et al. [1] and is synthesized by Zurek [2], Blume-Kohout and Zurek [3]. SBS provides a structural notion of objectivity [4], and a unifying review is Korbicz [5]. Strong-QD links entropic and structural conditions [6].

2. **Non-ideal environments and fragment size.** "Hazy" environments reduce redundancy and record capacity [7]. Photon-scattering models exhibit huge redundancy in everyday environments [10, 11].

3. **Hypothesis testing and optimal decoding.** Binary quantum hypothesis testing is classical material [12, 13]. The quantum Chernoff bound characterizes the optimal asymptotic error exponent [14, 15]. These tools are natural for QD because "learning the pointer value" is precisely a discrimination task between conditional fragment states.

We also connect to recent resource-theoretic and operational approaches emphasizing *accessible information* rather than mutual information [16].

3 Setup: SBS, ε-SBS, and observer quality

3.1 Spectrum Broadcast Structure and its approximation

Let S be the system and $\mathcal{E} = \mathcal{E}_1 \otimes \cdots \otimes \mathcal{E}_N$ a decomposition of the environment into fragments. We focus on a classical pointer random variable X taking values in a finite alphabet $\mathcal{X}$ (often $\mathcal{X} = \{0, 1\}$).

Definition 1 (SBS state)**.** A joint state $\sigma_{S\mathcal{E}}$ has *spectrum broadcast structure* (SBS) with respect to pointer basis $\{|x\rangle\}_{x\in\mathcal{X}}$ if it can be written as

$$\sigma_{S\mathcal{E}} = \sum_{x\in\mathcal{X}} p_x \, |x\rangle\langle x|_S \otimes \bigotimes_{k=1}^{N} \sigma_{\mathcal{E}_k}^{(x)}, \tag{1}$$

where p is a probability distribution and, for each fragment k, the conditional states $\{\sigma_{\mathcal{E}_k}^{(x)}\}_{x\in\mathcal{X}}$ have mutually orthogonal supports (perfect distinguishability) [4, 5].

Definition 2 (ε-SBS)**.** A state $\rho_{S\mathcal{E}}$ is *ε-SBS* if there exists an SBS state $\sigma_{S\mathcal{E}}$ such that

$$D_{\mathrm{tr}}(\rho_{S\mathcal{E}}, \sigma_{S\mathcal{E}}) \le \varepsilon, \qquad D_{\mathrm{tr}}(\rho, \sigma) := \tfrac{1}{2} \left\|\rho - \sigma\right\|_1 .$$

3.2 Observer quality

An observer interacts only with a subset of fragments and through an imperfect instrument.

Definition 3 (Observer quality)**.** An observer is specified by a quality triple

$$Q_O = (R_O, \Lambda_O, \tau_O),$$

where:

1. $R_O \in [0, 1]$ is an *access fraction*: out of N fragments, O can access at most $m_{\max} = \lfloor R_O N \rfloor$ fragments in a given observational episode;
2. Λ_O is a CPTP map acting on each accessed fragment, representing calibration noise, coarse-graining, or any pre-measurement processing;
3. τ_O is a temporal horizon (memory, stability, or acquisition time). In the central-spin model (Sec. 7), it is mapped to an acquisition time budget and a pointer-stability constraint.

When $\mathcal{X} = \{0, 1\}$, we can compress Λ_O to a scalar "single-fragment calibration" index.

Definition 4 (Binary calibration index)**.** Let ρ_0, ρ_1 be the two conditional states of a single accessed fragment after Λ_O, and assume equal priors. Define

$$C_O := 1 - P_e^\star(\rho_0, \rho_1), \qquad P_e^\star(\rho_0, \rho_1) = \tfrac{1}{2} \left(1 - \tfrac{1}{2} \left\|\rho_0 - \rho_1\right\|_1\right), \tag{2}$$

where $P_e^\star$ is the Helstrom-optimal single-copy Bayes error [12, 13]. Then $C_O \in [\frac{1}{2}, 1]$.

3.3 Observer inference topology: DLN instantiation in quantum Darwinism

The resource triple $Q_O = (R_O, \Lambda_O, \tau_O)$ parameterizes observer *limitations*—how many fragments can be accessed, how each is distorted, and how long coherence can be maintained. It does not parameterize the observer's *inference structure*: the topology by which evidence from multiple fragments is organized, combined, and—when necessary—reorganized.

The Dot–Linear–Network (DLN) framework [17] provides a graph-theoretic formalization of exactly this missing variable. DLN characterizes cognitive or information-processing stages by two objects: a *belief-dependency graph* G governing within-episode inference, and a *revision graph* $\mathcal{R}$ over a model space $\mathcal{M}$ governing when and how the active inference structure can be changed. We now show that both objects instantiate directly in the QD/SBS setting: G as the conditional-independence structure of the SBS state, and $\mathcal{R}$ as the set of physically realizable transitions between measurement strategies.

3.3.1 SBS states as bipartite factor DAGs (Level 1: belief graph G)

Proposition 1 (SBS conditional independence as a bipartite DAG)**.** *Let $\sigma_{S\mathcal{E}}$ be an SBS state (Definition 1) with pointer variable X taking values in $\mathcal{X}$. The tensor-product form*

$$\sigma_{S\mathcal{E}} = \sum_{x\in\mathcal{X}} p_x \, |x\rangle\langle x|_S \otimes \bigotimes_{k=1}^{N} \sigma_{\mathcal{E}_k}^{(x)} \tag{3}$$

defines a bipartite directed acyclic graph (DAG): a single latent node X with directed edges $X \to \mathcal{E}_k$ for $k = 1, \ldots, N$, and no edges among fragment nodes. Conditional on $X = x$, the fragment states $\{\sigma_{\mathcal{E}_k}^{(x)}\}_{k=1}^{N}$ are mutually independent:

$$\mathcal{E}_j \;\perp\!\!\!\perp\; \mathcal{E}_k \mid X \qquad \text{for all } j \neq k.$$

Proof. The product structure $\bigotimes_{k=1}^{N} \sigma_{\mathcal{E}_k}^{(x)}$ conditional on $X = x$ is the defining property of conditional independence in a tensor-product state. In the classical reduction (diagonal in the pointer basis, with each fragment traced to measurement outcomes y_k), the joint distribution factorizes as $p(x, y_1, \ldots, y_N) = p(x) \prod_k p(y_k \mid x)$, which satisfies the Markov property of the stated DAG: the pointer node X d-separates all fragment nodes [18]. □

Remark 1 (SBS as a DLN factor graph)**.** The DAG of Proposition 1 is precisely the *belief-dependency graph* G of a Network-stage agent in the DLN framework [17, Sec. 2.1]: a bipartite graph with F shared latent factors connected to K evidence nodes. In the QD setting, $F = |\mathcal{X}|$ (pointer alphabet size, typically $|\mathcal{X}| = 2$) and $K = N$ (number of environment fragments). Since QD objectivity requires high redundancy, i.e. $N \gg 1$, the condition $F \ll K$ that drives the DLN compression thesis is automatically and generically satisfied in any QD scenario.

3.3.2 Decoder classes as DLN stages

We define three nested classes of decoders on the m-fragment register, directly instantiating the DLN stage classification of [17, Sec. 2.1] in the QD measurement setting.

Definition 5 (Decoder classes (DLN stages in QD))**.** Let $A \subseteq \{1, \ldots, N\}$ with $|A| = m$, and let $\rho_A^{(x)} := \bigotimes_{k\in A} \Lambda_O(\sigma_{\mathcal{E}_k}^{(x)})$ denote the calibrated conditional states (SBS witness experiment, $\mathcal{X} = \{0, 1\}$). A *decoder* is a measurement–decision procedure producing an estimate $\widehat{X} \in \mathcal{X}$ from the m-fragment register. We define three decoder classes, each corresponding to a DLN stage [17, Sec. 2.1]:

(i) q_{D} **(Dot): memoryless decoding.** The decoder acts on at most one fragment $\mathcal{E}_k$ at a time and retains no state across fragments. The belief-dependency graph is empty ($G = \emptyset$): no evidence propagates between fragment nodes.

(ii) q_{L} **(Linear): product decoding with classical postprocessing.** The decoder applies a product POVM $M = \bigotimes_{k\in A} M_k$, followed by an arbitrary classical decision rule on the m outcomes. The belief-dependency graph is a null graph on m evidence nodes: each fragment is processed independently, and learning from fragment j does not update inference about fragment k.

(iii) q_{N} **(Network): collective decoding.** The decoder may apply an arbitrary joint POVM on the full register $\bigotimes_{k\in A} \mathcal{E}_k$. The belief-dependency graph is the bipartite DAG of Proposition 1: the observer's inference explicitly represents the pointer X as a shared latent parent of all fragment nodes, and evidence from any single fragment propagates through X to update predictions for all others.

Proposition 2 (Strict nesting of decoder classes)**.** *Let* Dec_D, Dec_L, Dec_N *denote the sets of all decoders in classes* q_{D}, q_{L}, q_{N}, *respectively. Then*

$$\mathsf{Dec}_D \subsetneq \mathsf{Dec}_L \subsetneq \mathsf{Dec}_N.$$

Both inclusions are strict whenever $m \geq 2$ *and the conditional fragment states* $\{\sigma_{\mathcal{E}_k}^{(x)}\}$ *are not identical across* x*.*

Proof. A single-fragment measurement on $\mathcal{E}_k$ is the product POVM with $M_j = \mathbf{1}$ for $j \neq k$, establishing $\mathsf{Dec}_D \subseteq \mathsf{Dec}_L$. Any product POVM is a special case of a joint POVM, giving $\mathsf{Dec}_L \subseteq \mathsf{Dec}_N$. For strictness of the first inclusion: any POVM acting on two or more fragments is in $\mathsf{Dec}_L \setminus \mathsf{Dec}_D$. For strictness of the second: the Helstrom-optimal measurement on $\rho_A^{(0)}$ versus $\rho_A^{(1)}$ is generically entangled across fragments when the per-fragment overlaps c_k are not 0 or 1 [12], placing it in $\mathsf{Dec}_N \setminus \mathsf{Dec}_L$. □

3.3.3 Quantitative content: stage-dependent error exponents and redundancy

The strict nesting of decoder classes has quantitative consequences for the central QD observable: the number of fragments required to achieve a given decoding error.

Proposition 3 (Tight exponent separation across DLN stages, pure-state records)**.** *Let* $|\psi_0\rangle, |\psi_1\rangle$ *be pure states with overlap* $c := |\langle\psi_0|\psi_1\rangle| \in (0,1)$*. Consider the task of discriminating* $|\psi_0\rangle^{\otimes m}$ *from* $|\psi_1\rangle^{\otimes m}$ *under equal priors. The optimal error exponents achievable by each decoder class are:*

$$\xi_{\mathrm{N}} := \lim_{m\to\infty} -\tfrac{1}{m}\log P_e^{\mathrm{coll}}(m) = -\log(c^2), \tag{4}$$

$$\xi_{\mathrm{L}} := \lim_{m\to\infty} -\tfrac{1}{m}\log P_e^{\mathrm{prod}}(m) = -\log(c), \tag{5}$$

$$\xi_{\mathrm{D}} := 0 \qquad \big(P_e^{\mathrm{single}} = \tfrac{1}{2}(1-\sqrt{1-c^2}),\ \textit{independent of } m\big). \tag{6}$$

In particular:

(a) The exponent ratio between Network and Linear stages is exactly 2*:* $\xi_{\mathrm{N}}/\xi_{\mathrm{L}} = 2$*.*

(b) Both exponents are achievable*:* ξ_{N} *by the Helstrom measurement on the joint* m*-copy register [14, 15], and* ξ_{L} *by the optimal single-copy POVM (which induces classical distributions with Bhattacharyya coefficient* $B = c$ *for pure states [19]) followed by the Neyman–Pearson likelihood-ratio test on the i.i.d. classical outcomes.*

(c) The Dot stage has zero exponent: a memoryless decoder's error is bounded below by the single-copy Helstrom error regardless of m, because no evidence is accumulated.

Proof. Equation (4) is the quantum Chernoff exponent for pure states [14, 15]. For (5): any single-copy POVM on pure states $|\psi_0\rangle, |\psi_1\rangle$ induces classical distributions p, q with Bhattacharyya coefficient $B(p,q) = \sum_y \sqrt{p(y)q(y)} \geq c$ [19, 20]. For the classical Chernoff coefficient, $\min_{s\in[0,1]} \sum_y p(y)^s q(y)^{1-s} \geq B$ (since $s = \frac{1}{2}$ is feasible and yields B), so the m-copy product-measurement coefficient is at least c^m, giving exponent at most $-\log c$. Achievability: the Helstrom single-copy POVM on pure states with overlap c induces classical distributions with $B = c$ exactly (direct calculation of the binary Bhattacharyya coefficient for the Helstrom outcome probabilities $p_\pm = \frac{1}{2}(1 \pm \sqrt{1-c^2})$), so the classical Chernoff exponent of the induced i.i.d. channel is precisely $-\log c$. Equation (6): a Dot decoder accesses one fragment per episode with no memory, so its error equals the single-copy Helstrom error irrespective of the total number of available fragments. □

Remark 2 (Mixed-state fragment records)**.** Proposition 3 is stated for pure-state records, which arise naturally in the central-spin worked example (Sec. 7) and in any pure-dephasing model. For mixed-state conditional fragment states, the exponent ratio ξ_N/ξ_L lies in $[1, 2]$: the lower bound 1 is saturated when the conditional states commute (classical records, where collective measurements offer no advantage over product measurements), and the upper bound 2 is saturated in the pure-state limit. We conjecture that the ratio is a monotone function of the non-commutativity of the conditional fragment states, interpolating continuously between the classical limit ($\xi_N/\xi_L = 1$ for commuting states) and the fully quantum limit ($\xi_N/\xi_L = 2$ for pure states). A natural candidate for the non-commutativity measure is the Hilbert–Schmidt distance to the nearest simultaneously diagonalizable pair, $d_{\mathrm{HS}}\big(\{\sigma^{(0)}, \sigma^{(1)}\}, \mathcal{C}_{\mathrm{comm}}\big)$, but verifying monotonicity of the exponent ratio with respect to this (or any other) measure requires controlling the s-optimization in the quantum Chernoff coefficient for non-commuting mixed states. A complete characterization of the mixed-state exponent gap in terms of the fragment state geometry—for instance, as a function of sandwiched Rényi divergences [21]—remains an open problem.

Corollary 1 (Stage-dependent redundancy requirement)**.** *Fix a target error $\delta \in (0, \frac{1}{2})$ and suppose all N fragments carry identical pure-state records with overlap c. Let $m_q(\delta)$ denote the minimum number of fragments sufficient for a stage-q observer to achieve error $\leq \delta$. To leading order in* $\log(1/\delta)$*:*

$$m_D = \infty \text{ (if } P_e^{\mathrm{single}} > \delta), \qquad m_L(\delta) \sim \frac{\log(1/(2\delta))}{-\log c}, \qquad m_N(\delta) \sim \frac{\log(1/(2\delta))}{-\log(c^2)} = \frac{m_L(\delta)}{2}.$$

A Network-stage observer requires half as many fragments as a Linear-stage observer for the same error target.

Proof. Immediate from Proposition 3 and the inversion $m_q(\delta) \sim \log(1/(2\delta))/\xi_q$. □

Remark 3 (Redundancy ratio as a DLN compression constant)**.** In the language of [17], the ratio $m_L/m_N = 2$ is the *compression efficiency gain*: the reduction in evidence units required when the observer exploits shared latent structure (the pointer variable) versus treating evidence units independently. This is the QD specialization of the $O(F)$-versus-$O(K)$ cost-scaling thesis of [17, Proposition 1(i)]. The ratio is an exact constant (not merely an asymptotic scaling relation) because the pointer alphabet size $|\mathcal{X}|$ is fixed while the number of fragments N grows, placing QD in the regime $F \ll K$ where the DLN compression advantage is maximal.

3.3.4 Model space and revision graph (Level 2: measurement-strategy transitions)

The DLN framework formalizes not only the within-episode belief structure (the graph G) but also the observer's capacity to *revise* that structure. Following [17, Sec. 2.3], this is captured by a model space $\mathcal{M}$ (the set of candidate belief structures) and a revision graph $\mathcal{R} = (\mathcal{M}, \mathcal{T})$ (a directed graph whose edges are the available transitions between structures). We now specialize these objects to the QD setting.

Definition 6 (Measurement model space)**.** For an observer O with resource triple $Q_O = (R_O, \Lambda_O, \tau_O)$, define the *measurement model space*

$$\mathcal{M}_O \subseteq \{\mathsf{Dec}_D,\ \mathsf{Dec}_L,\ \mathsf{Dec}_N\}$$

as the set of decoder classes that are physically realizable given Q_O. A decoder class Dec_q is in $\mathcal{M}_O$ if and only if the observer possesses the physical resources to implement at least one decoder in that class:

- $\mathsf{Dec}_D \in \mathcal{M}_O$ always (memoryless decoding requires no inter-fragment coherence).
- $\mathsf{Dec}_L \in \mathcal{M}_O$ whenever τ_O is sufficient to sequentially acquire m fragment outcomes and store classical records.
- $\mathsf{Dec}_N \in \mathcal{M}_O$ whenever τ_O is sufficient to maintain quantum coherence across the m-fragment register for the full acquisition-plus-decoding interval.

Definition 7 (Revision graph in QD)**.** The *revision graph* $\mathcal{R}_O = (\mathcal{M}_O, \mathcal{T}_O)$ is a directed graph over the observer's model space, where $\mathcal{T}_O \subseteq \mathcal{M}_O \times \mathcal{M}_O$ is the set of transitions the observer can execute. Following the DLN classification [17, Sec. 2.3]:

- **Dot.** $\mathcal{M}_O = \{\mathsf{Dec}_D\}$; $\mathcal{R}_O$ is a single vertex with no edges. No revision capacity.
- **Linear.** $\mathcal{M}_O = \{\mathsf{Dec}_L\}$; $\mathcal{R}_O$ is a single vertex. The observer occupies a fixed point in model space.
- **Network (expand-only).** $\mathcal{M}_O = \{\mathsf{Dec}_N, \mathsf{Dec}_L\}$ with a single directed transition $\mathsf{Dec}_N \to \mathsf{Dec}_L$ (degradation when coherence drops below the collective-decoding threshold). No return transition.
- **Network (full cycle).** Both transitions $\mathsf{Dec}_N \rightleftharpoons \mathsf{Dec}_L$ are available. $\mathcal{R}_O$ contains a directed cycle: the observer can degrade to product measurements when coherence is lost and recover collective measurements when coherence is restored.

Remark 4 (Physical mechanisms governing $\mathcal{R}$-transitions)**.** Transitions in $\mathcal{R}_O$ are governed by the relation between the observer's temporal horizon τ_O and the coherence time required for collective decoding. In laboratory settings, the relevant physical mechanisms include: (i) fluctuating dephasing rates (e.g., temperature-dependent T_2 in spin-bath experiments [22]), (ii) time-varying calibration noise (drift in detector efficiency or alignment), (iii) changes in pointer stability (system relaxation modifying the SBS quality parameter ε). An observer that monitors its own decoding performance—a Level 2 operation in the sense of [17, Sec. 2.3]—and switches decoder class in response, is executing a transition in $\mathcal{R}_O$.

Proposition 4 (Bounded recovery under measurement-strategy revision)**.** *Let an observer O initially operate in Dec_N (collective decoding, exponent $\xi_{\mathrm{N}} = -\log(c^2)$) and suppose coherence conditions degrade at time t_0, forcing a transition to Dec_L (product decoding, exponent $\xi_{\mathrm{L}} = -\log c$). Suppose coherence conditions subsequently recover at time $t_1 > t_0$.*

(i) If $\mathcal{R}_O$ contains the return transition $\mathsf{Dec}_L \to \mathsf{Dec}_N$ (full-cycle Network observer), the observer can recover the exponent ξ_{N} within a bounded verification interval after t_1. The recovery time is determined by the monitoring protocol (Level 2 overhead), analogous to the contraction bound in [17, Proposition 1(iii)].

(ii) If $\mathcal{R}_O$ lacks the return transition (expand-only Network observer), the observer remains at exponent ξ_{L} permanently, even after coherence is restored.

The performance cost of being locked in Dec_L is a factor of 2 in the required fragment count (Corollary 1):

$$m_{\mathrm{L}}(\delta) = 2\, m_{\mathrm{N}}(\delta) \qquad \textit{(pure-state records).}$$

Proof. Part (i): after coherence recovery, the conditions for $\mathsf{Dec}_N \in \mathcal{M}_O$ are again satisfied. A full-cycle observer with a Level 2 monitoring protocol (cf. the shadow-model verification of [17, Sec. 5.1]) detects that collective decoding is again feasible and executes $\mathsf{Dec}_L \to \mathsf{Dec}_N$. The verification interval is bounded by the monitoring window length plus a confirmation period, as established for the analogous contraction mechanism in [17, Proposition 1(iii)]. Part (ii): without the return transition, the observer has no mechanism to re-enter Dec_N, regardless of restored physical capacity. The fragment-count penalty follows from Corollary 1. □

Concrete monitoring protocol: coherence-gated decoder switching. We now specify a physically realizable Level 2 protocol for executing $\mathcal{R}$-transitions. The observer partitions its accessible fragments into a *decoding set* A_{dec} and a *monitoring set* A_{mon}, with $|A_{\mathrm{mon}}| = \lceil f \cdot m \rceil$ for a fixed monitoring fraction $f \in (0,1)$ (typically $f \approx 0.1$–0.2). The monitoring set is reserved for Level 2 diagnostics and does not contribute to the primary pointer estimate.

L2.1 Cross-validation scoring (continuous). In each observation episode: (a) apply the current decoder (collective or product) to A_{dec}, obtaining a pointer estimate $\widehat{x}$; (b) apply independent single-fragment measurements to each $\mathcal{E}_k \in A_{\mathrm{mon}}$, obtaining per-fragment estimates $\{\widehat{x}_k\}$; (c) compute the *consistency score* $s_t := |A_{\mathrm{mon}}|^{-1} \sum_{k \in A_{\mathrm{mon}}} \mathbf{1}[\widehat{x}_k = \widehat{x}]$. Maintain a rolling mean $\bar{s}_W$ over a window of the last W episodes.

L2.2 Expansion trigger ($\mathsf{Dec}_N \to \mathsf{Dec}_L$). If $\bar{s}_W$ falls below the *product-decoder baseline* $s_{\mathrm{prod}} := 1 - P_e^{\mathrm{single}}$ (the consistency expected when $\widehat{x}$ is no more reliable than majority vote over monitoring fragments), the collective decoder is no longer adding value beyond what product decoding achieves. The observer executes $\mathsf{Dec}_N \to \mathsf{Dec}_L$.

Physical trigger: equivalently, the observer may directly monitor its coherence time via a Ramsey-contrast or spin-echo sequence on an ancilla qubit coupled to the fragment register. If the estimated $\widehat{T}_2$ drops below the collective-decoding threshold $\tau_{\mathrm{coll}} := m\, t_{\mathrm{meas}} + t_{\mathrm{decode}}$, the transition is triggered.

L2.3 Contraction trigger ($\mathsf{Dec}_L \to \mathsf{Dec}_N$). While operating in Dec_L, the observer periodically runs a *shadow collective test* on a small subset $A_{\mathrm{shadow}} \subseteq A_{\mathrm{mon}}$ (with $|A_{\mathrm{shadow}}| \ll m$, requiring coherence only over the shadow subset): (a) apply a collective POVM to A_{shadow}, obtaining $\widehat{x}_{\mathrm{shadow}}$; (b) compare the shadow estimate's consistency with the product decoder's estimate over an evaluation window of length w. If the shadow collective measurement shows statistically significant improvement—specifically, if $\mathrm{MSE}_{\mathrm{shadow}} < (1-\theta)\,\mathrm{MSE}_{\mathrm{prod}}$ for a contraction margin $\theta \in (0,1)$—the observer executes $\mathsf{Dec}_L \to \mathsf{Dec}_N$.

Physical trigger: equivalently, if the re-estimated $\widehat{T}_2$ exceeds τ_{coll} for w consecutive episodes, the return transition is warranted.

Table 1: DLN instantiation in quantum Darwinism. The belief-dependency graph G (Level 1) and revision graph $\mathcal{R}$ (Level 2) are the formal objects of Wu [17]; the decoder class and error exponent are derived in this paper.

q_O	DLN stage	Belief graph G	Revision graph $\mathcal{R}$	QD decoder class	Exponent
q_{D}	Dot	$G = \emptyset$	$\lvert\mathcal{M}\rvert$=1; no edges	Single-fragment; memoryless	0
q_{L}	Linear	Null graph on m nodes	Fixed point	Product POVM $\bigotimes_k M_k$ + classical post.	$-\log c$
q_{N}	Network	Bipartite DAG: $X \to \mathcal{E}_k$	Cycle: $\mathsf{Dec}_N \rightleftharpoons \mathsf{Dec}_L$	Collective POVM on $\bigotimes_{k\in A} \mathcal{E}_k$	$-\log(c^2)$

The monitoring fraction f imposes an overhead: the effective decoding set is reduced to $(1-f)\,m$ fragments, increasing the required total fragment count by a factor of $1/(1-f)$ (e.g., $\sim$12% overhead for $f = 0.1$). This overhead is the Level 2 cost c_{meta} in the language of [17, Proposition 1]. The recovery time after coherence restoration is bounded by $n_{\mathrm{holdout}} + w$ episodes, where n_{holdout} is the minimum interval between contraction tests.

Remark 5 (Finite-resource sample complexity)**.** The fragment-count thresholds in Corollary 1 are leading-order (large-$\log(1/\delta)$) statements. For finite m, the non-asymptotic bounds of Secs. **??**–**??** (Chernoff upper bound, calibration contraction, ε-robustness) apply at each DLN stage. This places the stage distinction in the finite-resource regime of non-asymptotic quantum information theory [23–25].

4 Optimal decoding and Chernoff sample complexity

4.1 Binary hypothesis testing on fragments

Fix an SBS reference state $\sigma_{S\mathcal{E}}$ of the form (1) with $\mathcal{X} = \{0, 1\}$. For any fragment set $A \subseteq \{1, \ldots, N\}$, let

$$\sigma_A^{(x)} := \bigotimes_{k\in A} \sigma_{\mathcal{E}_k}^{(x)}$$

denote the conditional state of the accessible environment.

The observer first applies Λ_O to each accessed fragment and then performs an optimal measurement to decide x. This induces a binary quantum hypothesis testing problem:

$$H_0 :\ \rho_A = \bigotimes_{k\in A} \Lambda_O(\sigma_{\mathcal{E}_k}^{(0)}), \qquad H_1 :\ \rho_A = \bigotimes_{k\in A} \Lambda_O(\sigma_{\mathcal{E}_k}^{(1)}).$$

4.2 Quantum Chernoff bound and tight redundancy scaling

Define the (binary) quantum Chernoff coefficient for a pair of states ρ, σ:

$$Q(\rho, \sigma) := \min_{s\in[0,1]} \mathrm{Tr}\left[\rho^s \sigma^{1-s}\right],$$

and the associated Chernoff exponent

$$\xi(\rho, \sigma) := -\log Q(\rho, \sigma).$$

The quantum Chernoff bound states that for discriminating $\rho^{\otimes n}$ vs $\sigma^{\otimes n}$ with equal priors, the optimal error decays with exponent $\xi(\rho, \sigma)$ [14, 15].

We use a finite-n inequality that is convenient for sample-complexity statements.

Theorem 1 (Finite-n Chernoff upper bound)**.** *Let ρ, σ be density operators and consider equal priors on $H_0 : \rho$ and $H_1 : \sigma$. Then the optimal Bayes error obeys*

$$P_e^\star(\rho, \sigma) \leq \tfrac{1}{2}\, Q(\rho, \sigma). \tag{7}$$

Consequently, for product states over a fragment set A,

$$P_e^\star\left(\bigotimes_{k\in A} \rho_k, \bigotimes_{k\in A} \sigma_k\right) \leq \tfrac{1}{2} \min_{s\in[0,1]} \prod_{k\in A} \mathrm{Tr}\left[\rho_k^s \sigma_k^{1-s}\right].$$

Proof. Inequality (7) is a standard consequence of the Audenaert et al. bound and is commonly stated as $P_e^\star(\rho, \sigma) \leq \frac{1}{2} \min_{s\in[0,1]} \mathrm{Tr}[\rho^s \sigma^{1-s}]$ [14]. The product form follows from multiplicativity of the trace under tensor products. □

Definition 8 (Observer-effective Chernoff exponent on a fragment set)**.** For an observer O and fragment set A, define

$$\xi_O(A) := \max_{s\in[0,1]} \left(-\sum_{k\in A} \log \mathrm{Tr}\left[\Lambda_O(\sigma_{\mathcal{E}_k}^{(0)})^s\, \Lambda_O(\sigma_{\mathcal{E}_k}^{(1)})^{1-s}\right] \right). \tag{8}$$

Proposition 5 (Access threshold as an information budget)**.** *Fix an error target $\delta \in (0, \frac{1}{2})$ and an SBS reference experiment. If an observer can access at most $m_{\max} = \lfloor R_O N \rfloor$ fragments, then a sufficient condition for δ-decoding of the pointer value is the existence of a set A with $|A| \leq m_{\max}$ such that*

$$\xi_O(A) \geq \log\left(\frac{1}{2\delta}\right).$$

Proof. By Theorem 1, $P_e^\star(A) \leq \frac{1}{2} \exp(-\xi_O(A))$. If $\xi_O(A) \geq \log(1/(2\delta))$, then $P_e^\star(A) \leq \delta$. □

4.3 Calibration as distinguishability contraction

A central point for "non-ideal observers" is that calibration noise cannot improve distinguishability. For the Chernoff coefficient, this is a data-processing statement.

Theorem 2 (Calibration degrades Chernoff distinguishability)**.** *Let Λ be a CPTP map and ρ, σ quantum states. For every $s \in [0, 1]$,*

$$\mathrm{Tr}\left[\Lambda(\rho)^s \Lambda(\sigma)^{1-s}\right] \;\geq\; \mathrm{Tr}\left[\rho^s \sigma^{1-s}\right].$$

Equivalently, $Q(\Lambda(\rho), \Lambda(\sigma)) \geq Q(\rho, \sigma)$ and therefore

$$\xi(\Lambda(\rho), \Lambda(\sigma)) \leq \xi(\rho, \sigma).$$

Proof. For $s \in (0, 1)$, define the Petz-Rényi divergence $D_s(\rho\|\sigma) = \frac{1}{s-1} \log \mathrm{Tr}[\rho^s \sigma^{1-s}]$. For $s \in (0, 1)$ this divergence satisfies the data-processing inequality $D_s(\Lambda(\rho)\|\Lambda(\sigma)) \leq D_s(\rho\|\sigma)$ under CPTP maps [21, 23, 26]. Rearranging yields the claimed inequality for $\mathrm{Tr}[\cdot]$. The endpoint cases $s = 0, 1$ follow by continuity. □

5 ε-SBS robustness of decision rules

The point of an explicit trace-distance SBS approximation is that it immediately controls *any* decision procedure via data processing.

Lemma 1 (Decision-theoretic continuity under trace distance)**.** *Let ρ and σ be two states on the same Hilbert space and let* Dec *be any (possibly adaptive) measurement-plus-decision procedure outputting a discrete hypothesis $\widehat{X}$. Then*

$$\left|\mathbb{P}_\rho(\widehat{X} \neq X) - \mathbb{P}_\sigma(\widehat{X} \neq X)\right| \leq D_{\mathrm{tr}}(\rho, \sigma).$$

Proof. A measurement-plus-decision procedure is a CPTP map from states to a classical distribution on $\widehat{X}$. Trace distance contracts under CPTP maps, so the total variation distance between the induced classical distributions is bounded by $D_{\mathrm{tr}}(\rho, \sigma)$ [13]. The error event $\{\widehat{X} \neq X\}$ is a measurable subset of outcomes, hence its probability differs by at most the total variation distance. □

Theorem 3 (ε-robust Chernoff sample complexity)**.** *Let $\rho_{S\mathcal{E}}$ be ε-SBS with witness $\sigma_{S\mathcal{E}}$. Fix a fragment set A and an observer O. Let $\delta \in (0, \frac{1}{2})$ be a target error under the* actual *state ρ.*

If $\xi_O(A) \geq \log\left(\frac{1}{2(\delta-\varepsilon)}\right)$ and $\delta > \varepsilon$, then there exists a decision procedure on A (namely the optimal decoder for the witness experiment) such that

$$\mathbb{P}_\rho(\widehat{X} \neq X) \leq \delta.$$

Proof. Apply Proposition 5 to the witness state σ: with the given $\xi_O(A)$, there exists a decoder achieving $\mathbb{P}_\sigma(\widehat{X} \neq X) \leq \delta - \varepsilon$. Then Lemma 1 gives $\mathbb{P}_\rho(\widehat{X} \neq X) \leq (\delta - \varepsilon) + \varepsilon = \delta$. □

6 Local versus collective decoding: scope and a useful special case

Observer temporal limitations often restrict *which measurements are feasible*. A common distinction is between collective measurements across m fragments (which may require preserving quantum coherence across acquisition and decoding) and individual/product strategies (measuring each fragment immediately).

It is important to separate (i) what is true for *optimal* individual (non-entangling) strategies and (ii) what is true under additional local readout restrictions.

Proposition 6 (No universal exponent gap for two pure hypotheses)**.** *Let $|\psi_0\rangle$ and $|\psi_1\rangle$ be two pure states with overlap $c := |\langle\psi_0|\psi_1\rangle| \in (0, 1)$. For discriminating m copies with equal priors, there exist individual (non-entangling) measurement strategies whose error exponent matches the collective optimum, and adaptive individual strategies can match the exact multi-copy Helstrom error for every m [27].*

Remark 6 (A simple fixed individual measurement achieving the collective Chernoff exponent)**.** Projecting each copy onto the basis $\{|\psi_0\rangle, |\psi_0^\perp\rangle\}$ and deciding "1" if any $|\psi_0^\perp\rangle$ outcome occurs yields Bayes error $P_e = \frac{1}{2}c^{2m}$. This achieves the collective Chernoff exponent $-\log(c^2)$ (though not the optimal finite-m prefactor).

Although there is no *unconditional* exponent separation between product and collective measurements for two pure hypotheses, the situation is richer for mixed-state hypotheses or more than two hypotheses, where *strict* exponent separations can persist even for optimal local strategies [28, 29]. In the pure-state binary case, a constant-factor penalty does arise for certain widely used local readouts. One example is repeated application of the *single-copy Helstrom measurement* (the Bayes-optimal measurement for one copy) followed by optimal classical postprocessing.

Corollary 2 (Factor-of-two penalty for repeated single-copy Helstrom readout on pure records)**.** *Let $|\psi_0\rangle, |\psi_1\rangle$ be pure with overlap $c \in (0,1)$ and equal priors. If the observer measures each copy using the single-copy Helstrom POVM and then performs the optimal classical decision rule on the m outcomes, the achieved Chernoff exponent equals $-\log c$ per copy. By contrast, collective decoding achieves exponent $-\log(c^2)$ per copy. Thus, under this* fixed local readout restriction*, the collective exponent is exactly twice the Helstrom-repeated exponent.*

Proof. For a single copy, the Helstrom-optimal Bayes error for two pure states with overlap c (equal priors) is $P_e^{(1)} = \frac{1}{2}\big(1 - \sqrt{1-c^2}\big)$. The Helstrom measurement produces a symmetric binary channel with conditional outcome distributions $[1 - P_e^{(1)}, P_e^{(1)}]$ and $[P_e^{(1)}, 1 - P_e^{(1)}]$. For such symmetric binary distributions, the classical Chernoff coefficient is attained at $s = 1/2$ and equals $2\sqrt{P_e^{(1)}(1 - P_e^{(1)})} = c$. Thus the achievable product-measurement Chernoff exponent equals $-\log c$ per copy. Collective decoding attains the quantum Chernoff exponent $-\log(c^2)$ per copy for pure states. □

Remark 7 (Interpretation for observer quality)**.** Temporal limits (small τ_O) can motivate immediate per-fragment readout. However, for two pure hypotheses, optimal individual strategies can still match collective exponents (Proposition 6). Therefore, any performance gap must be attributed to additional observer constraints (e.g., fixed calibration/readout choices such as repeated single-copy Helstrom measurements), not to "locality" alone.

7 Worked physical model: central-spin pure dephasing

We now provide a concrete open-system model and compute (R_O, C_O, τ_O) in terms of physical parameters.

7.1 Model

Let S be a qubit with pointer basis the eigenbasis of σ_z^S. Let the environment consist of N qubits with $\sigma_z^{(k)}$. Consider the pure-dephasing Hamiltonian

$$H = \sigma_z^S \otimes \sum_{k=1}^{N} g_k \sigma_z^{(k)}, \tag{9}$$

and initial environment state $|+\rangle^{\otimes N}$ with $|+\rangle = (|0\rangle + |1\rangle)/\sqrt{2}$. Conditioned on the pointer value $x \in \{0,1\}$ (eigenvalues ± 1 of σ_z^S), fragment k evolves to a pure state

$$|\phi_k^{(x)}(t)\rangle = e^{\mp i g_k t \sigma_z} |+\rangle ,$$

so that the single-fragment overlap is

$$c_k(t) := \Big|\langle \phi_k^{(0)}(t)\rangle \, \phi_k^{(1)}(t)\Big| = |\cos(2g_k t)| . \tag{10}$$

This model (and its variants) is standard in decoherence theory and is directly connected to SBS formation in spin environments [5, 30].

7.2 Exact Chernoff exponent and fragment requirement

For pure states, the Chernoff coefficient equals the fidelity:

$$Q\left(|\phi_k^{(0)}(t)\rangle\,,|\phi_k^{(1)}(t)\rangle\right) = c_k(t)^2, \qquad \xi_k(t) = -\log c_k(t)^2.$$

For a set A of accessed qubits,

$$\xi(A;t) = \sum_{k\in A} -\log\left(\cos^2(2g_k t)\right), \tag{11}$$

and Theorem 1 implies

$$P_e^\star(A;t) \le \tfrac{1}{2}\exp(-\xi(A;t))\,.$$

Thus a sufficient condition for error $\le \delta$ is $\xi(A;t) \ge \log(1/(2\delta))$.

7.3 Mapping to observer parameters

Access fraction R_O. In a laboratory implementation, an observer may only intercept a fraction of environment qubits (geometric coverage, detector efficiency, spatial range). If $m_{\max}$ qubits are accessible per trial out of N, then $R_O = m_{\max}/N$.

Calibration C_O. Suppose the observer's instrument applies a depolarizing channel on each accessed environment qubit: $\Lambda_p(\rho) = (1-p)\rho + p\frac{\mathbf{1}}{2}$, capturing miscalibration or noise before readout. For any two qubit states, depolarization contracts trace distance by a factor $(1-p)$ [13]. For the central-spin conditional pure states, the single-copy Helstrom success probability becomes

$$C_O(t) = \tfrac{1}{2}\left(1 + (1-p)\sqrt{1-c_k(t)^2}\right) = \tfrac{1}{2}\left(1 + (1-p)|\sin(2g_k t)|\right),$$

where we used $c_k(t) = |\cos(2g_k t)|$. If couplings differ, $C_O(t)$ varies with k and can be summarized by a worst-case or average calibration across accessible fragments.

Temporal horizon τ_O. If the observer performs collective decoding across m fragments, a quantum memory must preserve coherence for at least the acquisition time of those m qubits plus the decoding time. Let t_{meas} be the per-qubit acquisition time. A minimal feasibility constraint is $\tau_O \gtrsim m\, t_{\text{meas}}$. Additionally, the pointer value must remain stable over the acquisition interval, typically limited by system relaxation times (e.g., T_1) [22, 31]. In this model, we treat stability as an explicit constraint rather than imposing an unjustified "exponential stability" assumption.

7.4 Numerical illustration and reproducibility

The accompanying repository includes a script that samples couplings $\{g_k\}$, computes $\xi(A;t)$ for the best accessible subset under an access fraction R_O, and plots redundancy as a function of time t. This is included to make the "worked example" fully reproducible. Figure 1 shows a typical redundancy profile as a function of interaction time in this toy model.

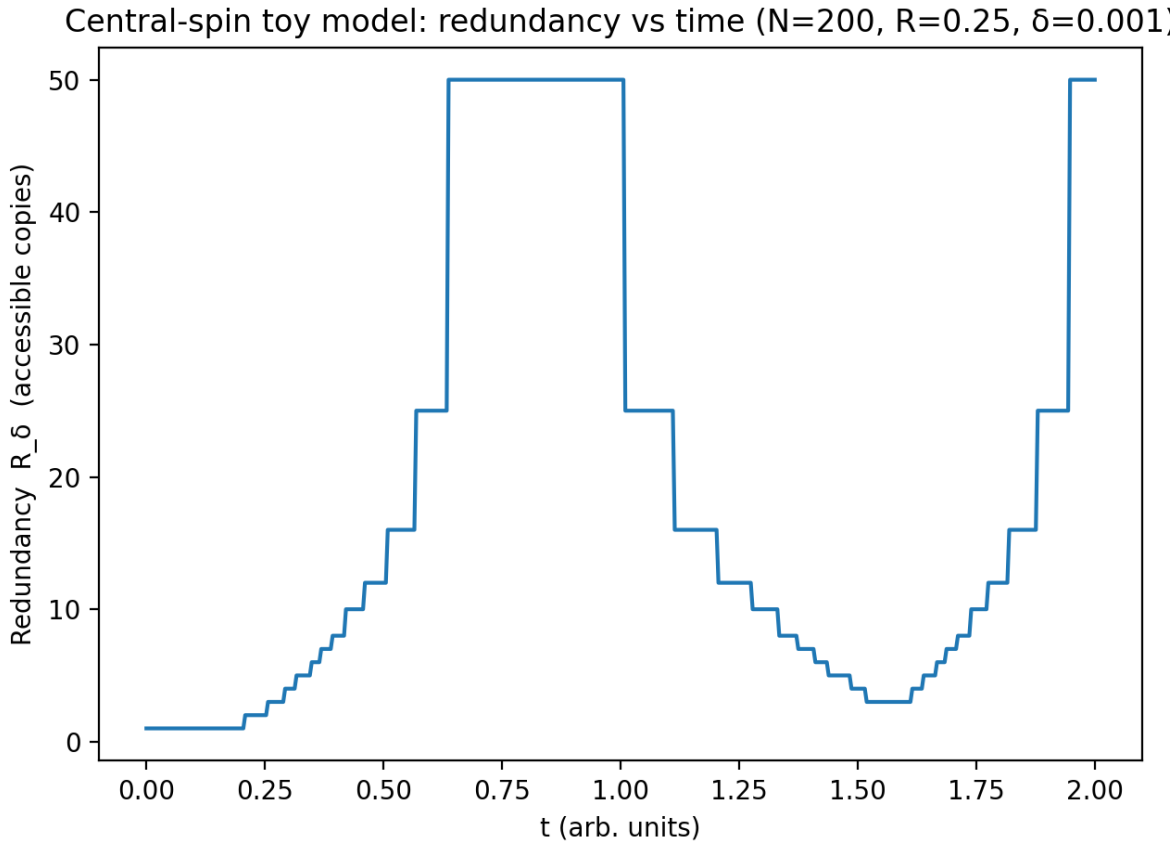

Figure 1: Central-spin toy model (Sec. 7): redundancy (accessible copies) versus interaction time t for a sampled distribution of couplings $\{g_k\}$, access fraction $R_O = 0.25$, and target decoding error $\delta = 10^{-3}$. The curve is produced by the reproducibility script in the repository.

8 DLN-series connection

The DLN instantiation developed in Sec. 3.3 imports the two formal objects of the DLN compression model—the belief-dependency graph G and the revision graph $\mathcal{R}$—and shows that they specialize to the QD/SBS setting without modification: G is the conditional-independence DAG of the SBS state (Proposition 1), and $\mathcal{R}$ is the directed graph of physically realizable transitions between measurement strategies (Definition 7).

The quantitative results of this paper fill in the *physics content* of each DLN stage in the quantum setting. The factor-of-two exponent gap (Proposition 3) is the QD expression of the $O(F)$-vs-$O(K)$ compression thesis of [17, Proposition 1(i)], and the bounded-recovery result (Proposition 4) is the QD expression of the return-transition mechanism of [17, Proposition 1(iii)].

We emphasize three points regarding scope:

1. The quantitative claims (Chernoff sample complexity, calibration contraction, ε-robustness) are self-contained and do not presuppose any developmental or cognitive interpretation of DLN.

2. The DLN framework provides the *structural classification* (which decoder topology) and the *revision formalism* (when the observer switches); the present paper provides the *quantitative*

content (error exponents, fragment counts, robustness bounds) that populates each cell of that classification in a physical setting.

3. The treatment of non-stationary observation protocols—where $\mathcal{R}$-transitions are exercised in response to changing decoherence conditions—and connections to adaptive quantum metrology are deferred to subsequent work.

9 Inverted sophistication: when collective decoding underperforms

The decoder hierarchy $\mathsf{Dec}_L \subsetneq \mathsf{Dec}_N$ (Definition 5) guarantees that the *optimal* collective POVM achieves error no larger than the optimal product measurement. However, if an observer deploys a collective decoder *without monitoring coherence conditions*, decoherence during measurement can cause the collective strategy to underperform product decoding—an effect we call *inverted sophistication*.

9.1 Binary coherence-loss model

Model the observer's coherence reliability as follows. In each observation episode, with probability f_{coh} coherence is maintained and the collective POVM succeeds (error P_e^{coll}); with probability $1 - f_{\text{coh}}$ coherence fails and the measurement output is uninformative ($P_e = \frac{1}{2}$). The effective error of an unmonitored collective decoder is then

$$P_e^{\text{unmon}}(m) = f_{\text{coh}}\, P_e^{\text{coll}}(m) + (1 - f_{\text{coh}})\, \tfrac{1}{2}. \tag{12}$$

For large m, $P_e^{\text{coll}}(m) \to 0$ exponentially, so $P_e^{\text{unmon}} \to (1 - f_{\text{coh}})/2$—a constant floor. Meanwhile, the product decoder's error $P_e^{\text{prod}}(m) = \frac{1}{2}e^{-\xi_{\text{L}} m}$ continues to decrease. Thus for any $f_{\text{coh}} < 1$, there exists a critical fragment count m^* above which the product decoder achieves strictly lower error than the unmonitored collective decoder.

Equating $P_e^{\text{prod}}(m)$ with $P_e^{\text{unmon}}(m)$ yields the critical coherence fraction below which inversion occurs at fragment count m:

$$f^*(m) = \frac{P_e^{\text{prod}}(m) - \frac{1}{2}}{P_e^{\text{coll}}(m) - \frac{1}{2}}. \tag{13}$$

Since P_e^{coll} decays faster than P_e^{prod} by the factor-of-two exponent gap (Corollary 2), $f^*(m) \to 1$ as $m \to \infty$: the coherence margin required for unmonitored collective decoding to remain competitive shrinks to zero.

9.2 Robustness across decoherence models

The binary success/failure model above is the harshest form of observer-side decoherence. Two alternative models bracket realistic behavior:

- **Continuous exponent degradation.** Instead of binary collapse, coherence loss degrades the effective exponent continuously: $P_e = \frac{1}{2}e^{-f_{\text{coh}}\, \xi_{\text{N}} m}$. Inversion occurs at a model-independent threshold $f^* = \frac{1}{2}$, independent of m.
- **System-side depolarization.** If the fragment states themselves become mixed (each conditional state replaced by $f_{\text{coh}}\, |\phi_k^{(x)}\rangle\langle\phi_k^{(x)}| + (1 - f_{\text{coh}})\, \frac{I}{2}$), both collective and product decoders degrade symmetrically. No inversion occurs: the collective advantage persists for all $f_{\text{coh}} > 0$.

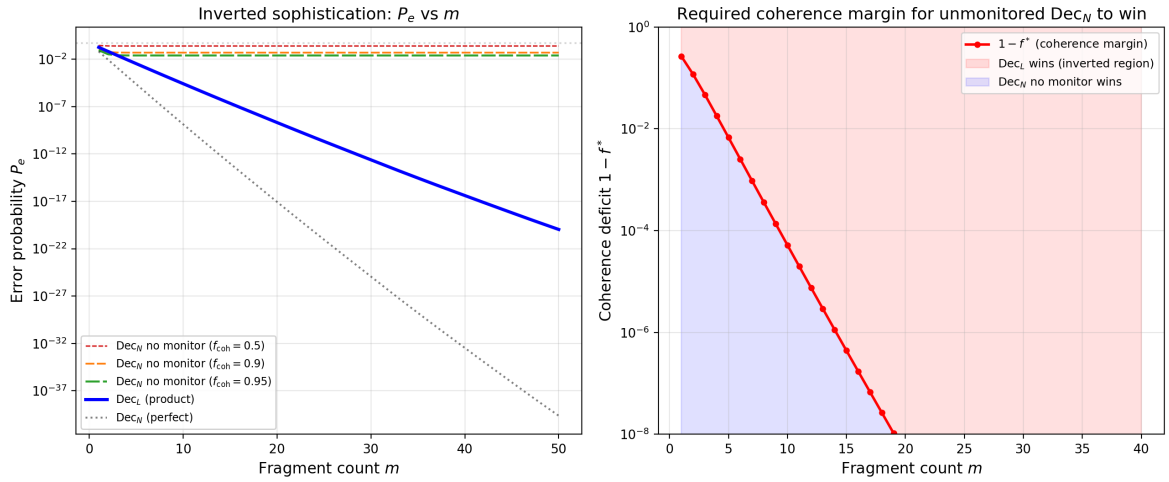

Figure 2: Inverted sophistication in the central-spin model. *Left:* Error probability vs. fragment count m for product decoding (Dec_L, solid blue) and unmonitored collective decoding (Dec_N, dashed) at three coherence fractions. At $f_{\mathrm{coh}} < 1$, the unmonitored collective error saturates at $(1 - f_{\mathrm{coh}})/2$ while Dec_L continues to improve. *Right:* Required coherence margin $1 - f^*$ vs. m (log scale). Above the curve (pink region), the product decoder achieves lower error; below (blue region), unmonitored collective decoding wins. The margin collapses exponentially with m.

The physical conclusion is that inverted sophistication requires *observer-side* decoherence (apparatus-level coherence failure), not *system-side* decoherence (environmental noise on the fragment states). This distinction maps directly onto the DLN revision-graph transitions of Sec. 8: the $\mathsf{Dec}_N \to \mathsf{Dec}_L$ downgrade triggered by coherence loss (L2.1) is precisely the scenario where inverted sophistication arises, and the monitoring protocol (L2.2–L2.3) restores the ability to adaptively choose the better decoder.

9.3 Central-spin illustration

Figure 2 illustrates the binary model for the central-spin parameters of Sec. 7. The left panel shows that at $f_{\mathrm{coh}} = 0.9$ the unmonitored collective decoder's error saturates at a floor of 0.05, while the product decoder continues to improve. The right panel shows $1 - f^*$ versus m: the coherence margin collapses exponentially, meaning that even 99.99% coherence reliability is insufficient at large m.

10 Discussion: tightness, limitations, and relation to prior work

We highlight three points relevant for interpreting the bounds and comparing to prior work:

- **Mathematical depth:** the main redundancy bound is phrased in terms of Chernoff-optimal decoding [14, 15] and explicitly incorporates calibration via a CPTP contraction theorem (Thm. 2) and ε-SBS perturbations (Thm. 3). The local-vs-collective decoding gap (Cor. 2) links temporal constraints to a provable reduction in error exponent.
- **Prior work:** we explicitly compare to hazy environments [7], photon redundancy [10, 11], generic objectivity [8, 9], and accessible-information approaches [16].

- **Concrete physical model:** Sec. 7 gives a full worked open-system example computing fragment overlaps and Chernoff exponents from Hamiltonian parameters.
- **DLN connection:** condensed to Sec. 8.

Scope and limitations. Several directions lie beyond the present analysis. (i) All sample-complexity bounds are stated for a *binary* pointer alphabet $\mathcal{X} = \{0, 1\}$; multi-hypothesis extensions require different Chernoff-type bounds and the factor-of-two exponent identity does not generalize straightforwardly. (ii) The central-spin model produces pure-state fragment records by construction (pure dephasing, no T_1 relaxation or system–environment back-action beyond decoherence). For mixed-state records—which are generic in realistic settings such as spin-boson models with loss or photon scattering at finite temperature—the collective/product exponent ratio lies in $[1, 2]$ and its precise dependence on non-commutativity remains open (Remark 2). (iii) The inverted sophistication threshold is quantitatively model-dependent: the binary observer-decoherence model (Model A) predicts $f^* \to 1$ exponentially in m, while the continuous model (Model B) gives $f^* = 1/2$ independently of m. Model B may be more physically representative in many experimental settings, and the binary model should be understood as an upper bound on the severity of the inversion effect. (iv) No experimental platform is analyzed in detail; connecting the observer-quality triple to specific detector architectures (e.g., NV centers, trapped ions, photonic QD setups) is an important next step for empirical validation.

11 Conclusion

Observer modeling is a structural gap in much of the QD/SBS literature. By treating the observer as a resource-constrained agent with explicit access, calibration, and temporal horizons, we obtain quantitative, decoder-level statements about redundancy and objectivity that remain stable under ε-SBS trace-distance approximations. The central-spin worked example demonstrates how these parameters can be computed from physical couplings and instrument noise, enabling model-to-experiment predictions. The factor-of-two exponent gap between local and collective decoding provides a sharp and testable link between temporal observer constraints and the emergence of objectivity. Moreover, the inverted-sophistication analysis (Sec. 9) shows that this link is fragile in practice: an unmonitored collective decoder can be strictly outperformed by product decoding when apparatus-level coherence reliability falls below a critical threshold that shrinks exponentially with fragment count, underscoring the necessity of coherence monitoring in the DLN revision-graph framework.

References

[1] Harold Ollivier, David Poulin, and Wojciech H. Zurek. Objective properties from subjective quantum states: Environment as a witness. *Physical Review Letters*, 93:220401, 2004. doi: 10.1103/PhysRevLett.93.220401.

[2] Wojciech H. Zurek. Quantum darwinism. *Nature Physics*, 5:181–188, 2009. doi: 10.1038/nphys1202.

[3] Robin Blume-Kohout and Wojciech H. Zurek. Quantum darwinism: Entanglement, branches, and the emergent classicality of redundantly stored quantum information. *Physical Review A*, 73:062310, 2006. doi: 10.1103/PhysRevA.73.062310.

[4] R. Horodecki, J. K. Korbicz, and P. Horodecki. Quantum origins of objectivity. *Physical Review A*, 91:032122, 2015. doi: 10.1103/PhysRevA.91.032122.

[5] J. K. Korbicz. Roads to objectivity: Quantum darwinism, spectrum broadcast structures, and strong quantum darwinism – a review. *Quantum*, 5:571, 2021. doi: 10.22331/q-2021-11-08-571.

[6] Thao P. Le and Alexandra Olaya-Castro. Strong quantum darwinism and strong independence are equivalent to spectrum broadcast structure. *Physical Review Letters*, 122:010403, 2019. doi: 10.1103/PhysRevLett.122.010403.

[7] Michael Zwolak, H. T. Quan, and Wojciech H. Zurek. Quantum darwinism in a hazy environment. *Physical Review Letters*, 103:110402, 2009. doi: 10.1103/PhysRevLett.103.110402.

[8] Fernando G. S. L. Brandão, Marco Piani, and Paweł Horodecki. Generic emergence of classical features in quantum darwinism. *Nature Communications*, 6:7908, 2015. doi: 10.1038/ncomms8908.

[9] Paul A. Knott, Tommaso Tufarelli, Marco Piani, and Gerardo Adesso. Generic emergence of objectivity of observables in infinite dimensions. *Physical Review Letters*, 121:160401, 2018. doi: 10.1103/PhysRevLett.121.160401.

[10] C. Jess Riedel and Wojciech H. Zurek. Quantum darwinism in an everyday environment: Huge redundancy in scattered photons. *Physical Review Letters*, 105:020404, 2010. doi: 10.1103/PhysRevLett.105.020404.

[11] C. Jess Riedel and Wojciech H. Zurek. Redundant information from thermal illumination: Quantum darwinism in scattered photons. *New Journal of Physics*, 13:073038, 2011. doi: 10.1088/1367-2630/13/7/073038.

[12] C. W. Helstrom. *Quantum Detection and Estimation Theory*. Academic Press, 1976.

[13] John Watrous. *The Theory of Quantum Information*. Cambridge University Press, 2018. ISBN 9781316848142.

[14] K. M. R. Audenaert, M. Nussbaum, A. Szkoła, and F. Verstraete. Discriminating states: The quantum chernoff bound. *Physical Review Letters*, 98:160501, 2007. doi: 10.1103/PhysRevLett.98.160501.

[15] Michael Nussbaum and Arleta Szkoła. The chernoff lower bound for symmetric quantum hypothesis testing. *The Annals of Statistics*, 37(2):1040–1057, 2009. doi: 10.1214/08-AOS593.

[16] Akram Touil, Bin Yan, Davide Girolami, Sebastian Deffner, and Wojciech Hubert Zurek. Eavesdropping on the decohering environment: Quantum darwinism, amplification, and the origin of objective classical reality. *Physical Review Letters*, 128:010401, 2022. doi: 10.1103/PhysRevLett.128.010401.

[17] A. Wu. Compression efficiency and structural learning as a computational model of dln cognitive stages. *bioRxiv*, 2026. doi: 10.64898/2026.02.01.703168.

[18] Judea Pearl. *Probabilistic Reasoning in Intelligent Systems: Networks of Plausible Inference*. Morgan Kaufmann, 1988.

[19] Christopher A. Fuchs and Carlton M. Caves. Ensemble-dependent bounds for accessible information in quantum mechanics. *Physical Review Letters*, 73:3047–3050, 1994. doi: 10.1103/PhysRevLett.73.3047.

[20] Richard Jozsa. Fidelity for mixed quantum states. *Journal of Modern Optics*, 41(12):2315–2323, 1994. doi: 10.1080/09500349414552171.

[21] Milán Mosonyi and Tomohiro Ogawa. Quantum hypothesis testing and the operational interpretation of the quantum rényi relative entropies. *Communications in Mathematical Physics*, 334:1617–1648, 2015. doi: 10.1007/s00220-014-2248-x.

[22] Maximilian Schlosshauer. *Decoherence and the Quantum-to-Classical Transition*. Springer, 2007.

[23] Marco Tomamichel. *Quantum Information Processing with Finite Resources: Mathematical Foundations*, volume 5 of *SpringerBriefs in Mathematical Physics*. Springer, 2016. ISBN 978-3-319-21890-8. doi: 10.1007/978-3-319-21891-5.

[24] Koenraad M. R. Audenaert, Milán Mosonyi, and Frank Verstraete. Quantum state discrimination bounds for finite sample size. *Journal of Mathematical Physics*, 53(12):122205, 2012. doi: 10.1063/1.4768252.

[25] Hao-Chung Cheng, Nilanjana Datta, Nana Liu, Theshani Nuradha, Robert Salzmann, and Mark M. Wilde. An invitation to the sample complexity of quantum hypothesis testing. *npj Quantum Information*, 11:94, 2025. doi: 10.1038/s41534-025-00980-8.

[26] Dénes Petz. Quasi-entropies for finite quantum systems. *Reports on Mathematical Physics*, 23 (1):57–65, 1986. doi: 10.1016/0034-4877(86)90067-4.

[27] Antonio Acín, Emilio Bagan, Maria Baig, Ll. Masanes, and Ramón Muñoz-Tapia. Multiple-copy two-state discrimination with individual measurements. *Physical Review A*, 71:032338, 2005. doi: 10.1103/PhysRevA.71.032338.

[28] John Calsamiglia, Julio I. de Vicente, Ramón Muñoz-Tapia, and Emilio Bagan. Local discrimination of mixed states. *Physical Review Letters*, 105:080504, 2010. doi: 10.1103/PhysRevLett.105.080504.

[29] Masaki Owari and Masahito Hayashi. Two-way classical communication remarkably improves local distinguishability. *New Journal of Physics*, 10:013006, 2008. doi: 10.1088/1367-2630/10/1/013006.

[30] Kamil Roszak and Jarosław K. Korbicz. Entanglement and objectivity in pure dephasing models. *Physical Review A*, 100:062127, 2019. doi: 10.1103/PhysRevA.100.062127.

[31] H.-P. Breuer and F. Petruccione. *The Theory of Open Quantum Systems*. Oxford University Press, 2002.